ADVANCED HEALTHCARE MATERIALS
www.advhealthmat.de

Mg–Al and Zn–Al Layered Double Hydroxides Promote Dynamic Expression of Marker Genes in Osteogenic Differentiation by Modulating Mitogen-Activated Protein Kinases

*Ha Ram Kang, Célio Junior da Costa Fernandes, Rodrigo Augusto da Silva, Vera Regina Leopoldo Constantino, Ivan Hong Jun Koh, and Willian F. Zambuzzi**

The effect of LDH samples comprised of chloride anions intercalated between positive layers of magnesium/aluminum (Mg-Al LDH) or zinc/aluminum (Zn-Al LDH) chemical composition on pre-osteoblast performance is investigated. Non-cytotoxic concentrations of both LDHs modulated pre-osteoblast adhesion by triggering cytoskeleton rearrangement dependent on recruiting of Cofilin, which is modulated by the inhibition of the Protein Phosphatase 2A (PP2A), culminating in osteoblast differentiation with a significant increase of osteogenic marker genes. The alkaline phosphatase (*ALP*) and bone sialoprotein (*BSP*) are significantly up-modulated by both LDHs; however, Mg-Al LDH nanomaterial promoted even more significance than both experimental controls, while the phosphorylations of mitogen-activated protein kinase (MAPKs)- extracellular signal–regulated kinases (ERK) and c-Jun N-terminal kinase (JNK) significantly increased. MAPK signaling is necessary to activate Runt-related transcription factor 2 (*RUNX2*) gene. Concomitantly, it is also investigated whether challenged osteoblasts are able to modulate osteoclastogenesis by investigating both osteoprotegerin (*OPG*) and Receptor activator of nuclear factor kappa-ligand (*RANKL*) in this model; a dynamic reprogramming of both these genes is found, suggesting LDHs in modulating osteoclastogenesis. These results suggest that LDHs interfere in bone remodeling, and they can be considered as nanomaterials in graft-based bone healing or drug-delivery materials for bone disorders.

1. Introduction

Bone defects are one of the most pressing problems in the medical–dental area.[1,2] Reconstruction of injured tissue is one of the greatest challenges for surgeons, and application of a biomaterial is often necessary for adequate tissue regeneration.[3] Specific to bone, the therapeutic biomaterial should have osteopromotive characteristics, which facilitate the differentiation of undifferentiated cells in mature osteoblasts.[4] In turn, osteoblasts are a terminally differentiated form of pre-osteoblasts (pre-Obs) and are responsible for bone formation by sequentially producing bone matrix proteins, which subsequently induce tissue mineralization.[5,6]

Layered double hydroxides (LDHs) can be described as a class of inorganic materials 2D organized with anion exchange properties and an interesting equilibrium between chemical stability and biodegradability. A synthetic LDH with composition $[Mg_6Al_2(OH)_{16}]CO_3 \cdot 4H_2O$, and known as hydrotalcite, is used commercially as the antacid Talcid.[7] In the 1990s, several papers showed the efficacy of Talcid compared to other antacids already well known in the market through in vitro and in vivo tests.[8–10] These studies showed the efficacy of hydrotalcite in the gastric mucosal protection, angiogenesis activation of wounded mucosa, healing of gastroduodenal ulcers, and progress in the aspect of mucosal scar. In addition to its acid neutralization effect, Talcid can activate genes for epidermal growth factor as well as its receptor in normal and ulcerated gastric mucosa.

LDHs exhibit the $[M^{II}_{(1-x)}M^{III}_x(OH)_2]^{x+}(A^{m-})_{x/m}.nH_2O$ general formula where M^{II} and M^{III} are di- and trivalent cations

H. R. Kang, C. J. da Costa Fernandes, R. A. da Silva, Prof. W. F. Zambuzzi
Laboratorio de Bioensaios e Dinâmica Celular
Departamento de Química e Bioquímica
Instituto de Biociências
Universidade Estadual Paulista–UNESP
campus Botucatu, São Paulo CEP 18618-970, Brazil
E-mail: wzambuzzi@ibb.unesp.br

The ORCID identification number(s) for the author(s) of this article can be found under https://doi.org/10.1002/adhm.201700693.

DOI: 10.1002/adhm.201700693

V. R. L. Constantino
Departamento de Química Fundamental
Instituto de Química
Universidade de São Paulo–USP
Av. Prof. Lineu Prestes 748, São Paulo CEP 05508-000, Brazil
Prof. I. H. J. Koh
Departamento de Cirurgia
Universidade Federal de São Paulo–UNIFESP
Rua Botucatu 740, CEP 04023-900 São Paulo, Brazil

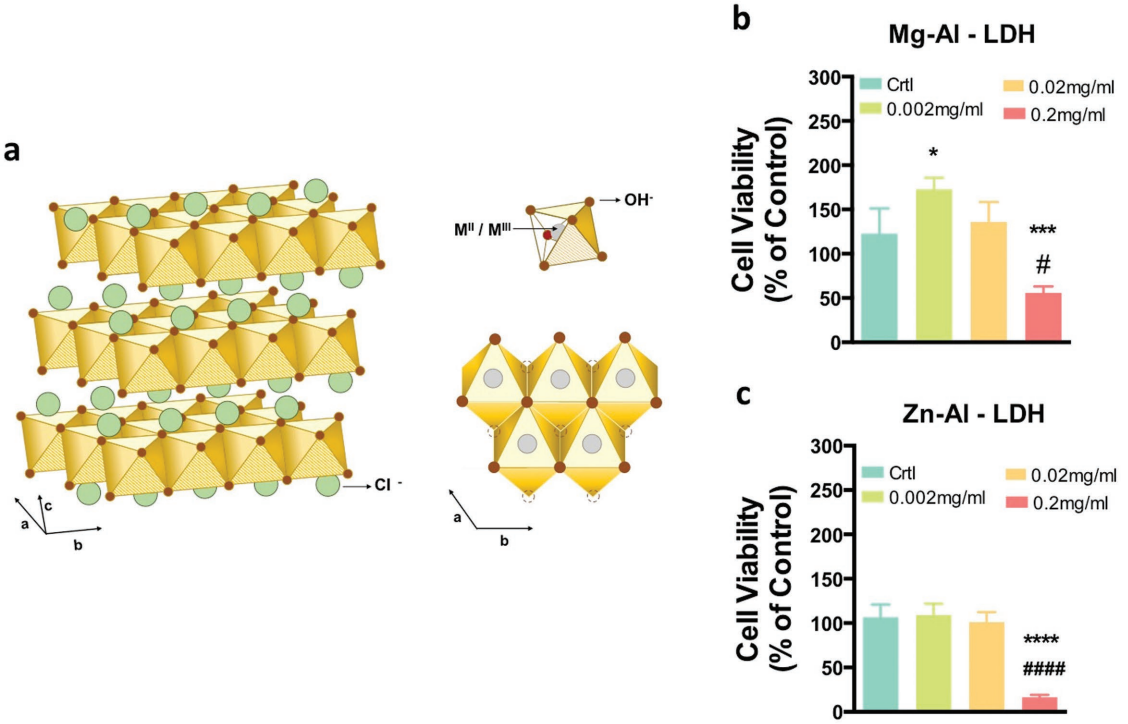

Figure 1. Schematic representation of LDH structures and their cytotoxicity. a) Each octahedral unit has six hydroxide ions coordinated to the metal cation in the central site; each hydroxide ion is shared by three octahedrons (or three metal ions). The layers are in [*ab*] plane while assembling of the layers is accomplished in the *c* axis direction. To investigate the cytotoxic effect of LDHs, pre-Obs were plated and in the semiconfluence were subjected with different concentrations of LDHs, as shown. Pre-Obs were treated with conventional medium for the control group; b) Mg–Al LDH diluted in three different concentrations (0.002; 0.02; 0.2 mg) and c) Zn–Al LDH diluted in three different concentrations (0.002; 0.02; 0.2 mg). $*p < 0.05$; $***p < 0.0002$; $****p < 0.0001$: Significant statistical difference when compared to control; $\#p < 0.05$; $\#\#\#\#p < 0.0001$: Significant statistical difference when comparing Mg_2Al–Cl 0.2 mg and Mg_2Al–Cl 0.02–0.002 mg.

positioned in octahedral $[M(OH)_6]$ units share edges in an layered fashion (**Figure 1**a), while A represents an anion of valence *m* that is sandwiched between the layers, neutralizing their electrical positive charges (simplified notation is $M^{II}{}_RM^{III}$–A, where *R* is the M^{II}/M^{III} molar ratio).[11] Usually, the interlayer spaces and the external surfaces of LDHs are occupied by water molecules. The distance between the stacking layers can be modified to accommodate anions of different sizes, electrical charges, and chemical nature (inorganic or organic).

Considering the possibility of controlling the chemical composition of LDH layers and their affinity for anions, drugs, and other biological bioactive species, they have been confined between the inorganic layers for drug delivery and imaging.[12–15] Our group has been studying experimental parameters for the intercalation of drugs such as pravastatin[16] and sulindac into LDHs and applying structural, spectroscopic, textural, and thermal techniques for their detailed characterization.[17,18] We recently reported the biological properties of a LDHs intercalated with the anion of mefenamic acid evaluated through the in vitro cytotoxicity tests by hemolysis, and in vivo tests concerning the anti-inflammatory activity and nociceptive effect of the intercalated and nonintercalated drug.[19] The mefenamate confinement in the LDH structure decreased its hemolytic effect and potentiated its anti-inflammatory and analgesic effects. In another study, the biocompatibility of LDH containing magnesium and zinc as divalent as aluminum as trivalent metal (chloride as intercalated anion) was investigated by histology and microcirculatory dynamic imaging, through sidestream dark field imaging, after implantation into the abdominal wall of rats.[20] Remarkable biocompatibility, rapid induction of fibroblast proliferation, neovascularization, and subsequent collagen production in vivo assays were observed.

Studies focusing on the action of LDHs on bone cells are very scarce.[21,22] Hence, we investigated the effect of LDH materials on preosteoblast metabolism, mainly addressing their possibility to modulate the expression of osteogenic differentiation genes. Summarizing, our results showed that both LDHs assayed here were able to modulate osteoblast metabolism, further compromising osteoclastogenesis. Importantly, we report for the first time, the acquisition of osteogenic phenotype by LDHs in a mitogen-activated protein kinase (MAPK)-dependent manner. Thus, these results suggest LDHs as very interesting nanomaterials to be explored in bone bioengineering as a scaffold or drug-delivery materials for bone disorders.

2. Results

LDH samples were prepared and characterized as previously described.[12] According to data analysis, the chemical

formulae $[Mg_{2.10}Al(OH)_{6.20}]Cl\cdot 2.3H_2O$ and $[Zn_{2.08}Al(OH)_{6.16}]Cl\cdot 1.7H_2O$ (abbreviated Mg_2Al–Cl and Zn_2Al–Cl) were proposed. Zeta potential measurements of the LDH suspensions in water gave the values +41.7 mV for Mg_2Al–Cl and +46 mV for Zn_2Al–Cl.

Thereafter, both LDH samples were diluted in cell culture medium (0.002, 0.02, and 0.2 mg mL^{-1}) to treat preosteoblasts in vitro to determine their cytotoxicity. After 24 h of treatment, the cell viability test was performed by 3-(4,5-dimethylthiazol-2-yl)-2,5-diphenyltetrazolium bromide (MTT) reduction (vital dye able to be reduced by mitochondrial dehydrogenases). This showed that cell viability decreased around 20% compared to control when the concentration of both LDHs was 0.2 mg mL^{-1} (Figure 1b,c). However, at 0.002 mg mL^{-1}, both LDHs did not present any cytotoxicity, but Mg_2Al–Cl promoted a significant increase of dehydrogenase activities (Figure 1b).

2.1. LDH Materials Affect Preosteoblast Adhesion by Modulating Cofilin and PP2A Phosphorylations

To evaluate the first effect of LDH on pre-Ob adhesion, the cells were subjected to both LDHs separately up to 24 h, then the cells were trypsinized, counted, and replated. After 3 and 24 h, the adherent cells were stained with violet crystal, which allowed us to estimate cell adhesion in response to LDH (**Figure 2**a,b). After the first 3 h of adhesion, LDH containing

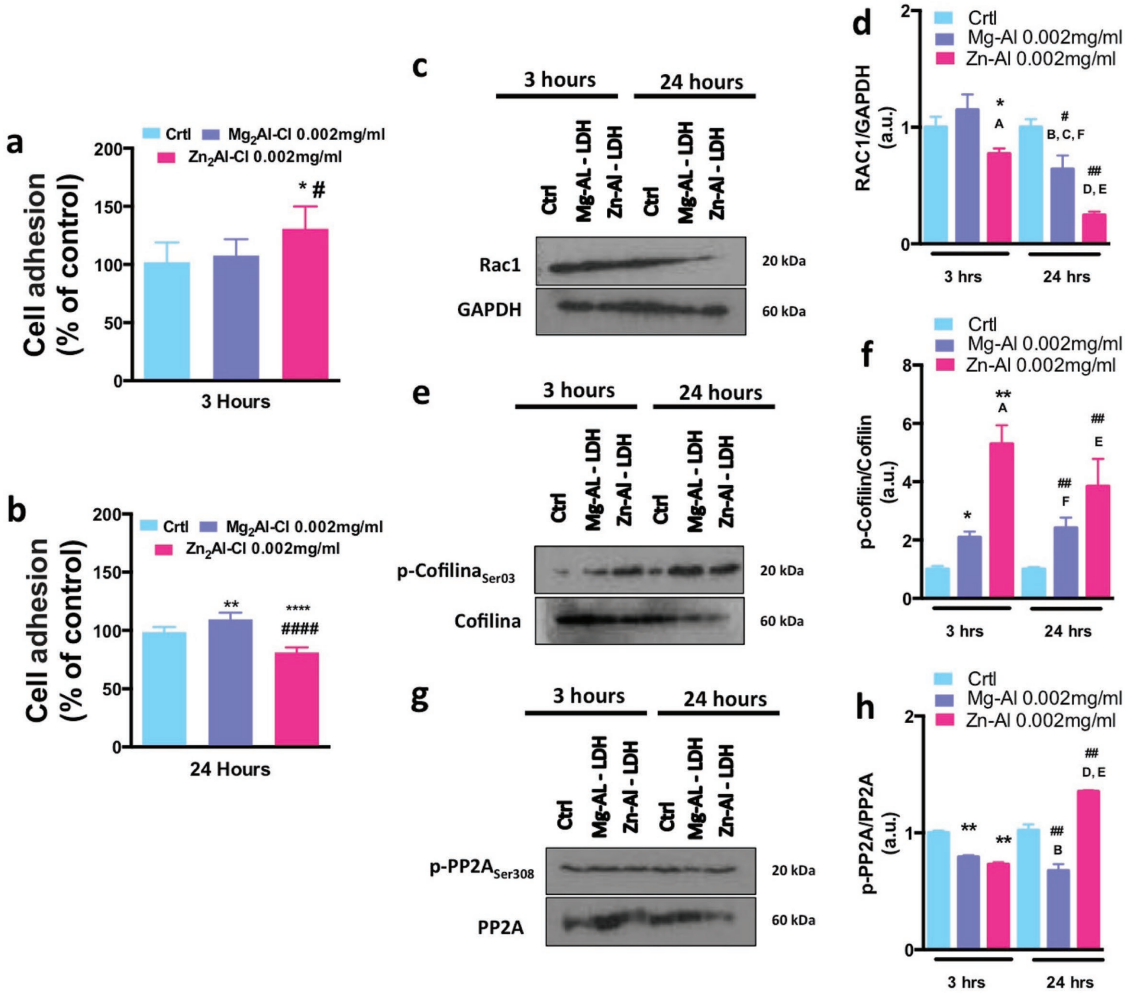

Figure 2. LDH impacts pre-Ob adhesion by modulating Cofilin/PP2A balance. Pre-Ob maintained with conventional medium was the control group. a,b) First, cell adhesion was measured by vital violet crystal after 3 and 24 h of plating, where treatments were made at a concentration of 0.002 mg mL^{-1}, as suggested previously as a subtoxic concentration. Thereafter, immunoblots showed the profile of phosphorylation of cofilin and PP2A, and Rac-1 expression. Representative results are depicted and the graphs represent arbitrary values obtained by a densitometric analysis of bands normalized by the mean values of the respective GADPH (internal control) bands. c,d) Expression analysis of Rac1; e,f) analysis of p-Cofilin/Cofilin ratio; and g,h) analysis of the expression of p-PP2A/PP2A ratio. Statistical significances were considered when: $^{**}p < 0.0017$; $^{***}p < 0.0002$; $^{****}p < 0.0001$:. $\#p < 0.05$; $\#\#\#\#p < 0.0001$. Statistical significances were considered when comparing Mg_2Al–Cl 0.2 mg and Mg_2Al–Cl 0.02–0.002 mg. (a) $p < 0.05$: Significant statistical difference when comparing Mg_2Al–Cl 3 h and Zn_2Al–Cl 3 h. (b) $p < 0.05$: Significant statistical difference when comparing Mg_2Al–Cl 24 h and Zn_2Al–Cl 24 h. (c) Significant statistical difference when comparing Mg_2Al–Cl 3 h and Mg_2Al–Cl 24 h. (d) $p < 0.0017$: Significant statistical difference when comparing Zn_2Al–Cl 3 h and Zn_2Al–Cl 24 h. (e) $p < 0.0002$: Significant statistical difference when comparing Mg_2Al–Cl 3 h and Zn_2Al–Cl 24 h. (f) Significant statistical difference when comparing Zn_2Al–Cl 3 h and Mg_2Al–Cl 24 h.

Zn^{2+} (Zn_2Al–Cl) significantly upmodulated pre-Ob adhesion, while cells treated with Mg^{2+} (Mg_2Al–Cl) remained unchanged. After 24 h, the same procedure was carried out, and LDHs produced an inverse effect; Mg_2Al–Cl upmodulated pre-Ob adhesion, Zn_2Al–Cl downmodulated it (Figure 2a,b).

Later, we investigated how the molecular machinery was involved during pre-Ob adhesion at 3 and 24 h, mainly with regard to the signaling protein involved with cytoskeleton rearrangement, which was previously proposed to be a pre-Ob adhesion biomarker.[23–25] Our results found that Rac-1 decreased in response to both evaluated LDHs at both chosen experimental times (Figure 2c,d).

Additionally, the phosphorylation of Cofilin significantly increased in response to both LDHs, with very similar phosphorylation profile at both 3 and 24 h (Figure 2e,f). Zn_2Al–Cl produced a more significant response, which was greater at 3 h than at 24 h (Figure 2e,f). The Mg-doped LDHs produced a similar response at both 3 and 24 h, which were significantly different than control (Figure 2e,f).

Finally, we investigated the involvement of PP2A, a very important Ser/Thr phosphatase able to modulate Cofilin phosphorylation balance by hydrolyzing the phosphoryl moiety from the phosphorylated protein, during pre-Ob adhesion. The phosphorylation of PP2A was assayed at Y307, a well-known inhibitory phosphorylation site of PP2A. Our results showed that the phospho-PP2A/PP2A ratio was decreased at 3 h of cell adhesion in response to both the LDHs assayed (Figure 2g,h). However, at 24 h, it was significantly increased in response to Zn_2Al–Cl (Figure 2g,h).

2.2. LDH Materials Require MAPK Activations during Osteogenic Pathway

Next, we focused on the possibility that LDHs promote pre-Ob differentiation. We experimentally treated pre-Ob with both the LDH nanohybrids, separately up to 14 d, when it was possible to determine the osteogenic phenotype, as detailed elsewhere. After 14 d, biological samples were collected and used for different technologies. First, we focused on understanding whether AKT and MAPKs are required in response to LDHs. MAPKs in osteoblasts are critical transducers able to maintain bone mass.[26] Our result clearly showed that phosphorylation of AKT was downregulated, but required, in response to both LDH materials (**Figure 3**a,b). The very similar profile was also seen in response to the positive control, where the cells were treated with osteogenic medium. Importantly, both MAPKs p44/p42 extracellular signal-regulated kinase (ERK)

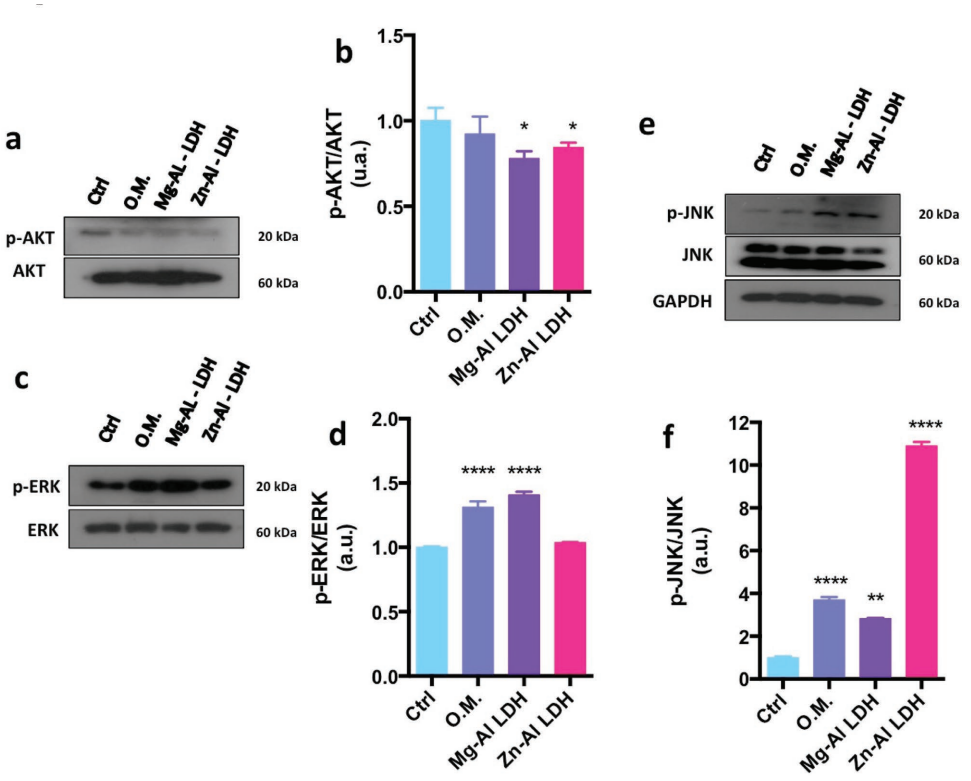

Figure 3. LDHs promote osteoblastic differentiation by upactivating both MAPKs – ERK and JNK. Pre-Obs were plated and at semiconfluence were treated with different experimental condition, as follows: control group, osteogenic medium (O.M.), Mg_2Al–Cl, and Zn_2Al–Cl. After 14 d of treatment, the cells were scraped then lysed using standard lysing buffer (as described in detail in the Experimental Section), and the pooled protein was resolved on SDS-PAGE gel. After polyvinylidene difluoride (PVDF) membrane transferring, cells were incubated using specific primary antibody in western blotting technology. The proteins investigated were: a,b) AKT; MAPKs c,d) ERK and e,f) JNK. Representative blottings are shown, and the graphs represent arbitrary values obtained by densitometric analysis of bands normalized by the average values of the respective GADPH bands (housekeeping control). $*p < 0.05$; $**p < 0.015$; $****p < 0.0001$: Significant statistical difference when compared to control.

(Figure 3c,d) and c-jun N-terminal kinase (JNK) (Figure 3e,f) were significantly upmodulated in response to both the LDH samples.

2.3. LDH-Induced Extracellular Matrix (ECM) Remodeling Requires Dynamic Matrix Metalloproteinases (MMPs) and Their Inhibitor Gene Reprograming

Additionally, we focused on understanding whether the ECM remodeling mechanism was modulated by LDH. We stained ECM cells with three different protocols to verify the behavior of the cells and in vitro-secreted extracellular matrix. Hematoxylin & eosin staining suggests a loose connective tissue in response to both LDH samples (**Figure 4**a), which was validated by Picrosirius red staining (Figure 4a,b). At this point, there was a significant staining on collagen fibers in response to both LDHs (Figure 4b), which was lower in response to Mg–Al LDH.

These results prompted us to investigate whether ECM remodeling-related genes were involved, and we found dynamic gene reprograming in response to both LDHs (Figure 4). ECM serves diverse functions and is a major component of the cellular microenvironment,[27] and its remodeling is mainly governed by MMPs and their tissue inhibitors (tissue inhibitors of matrix metalloproteinases (TIMPs) and reversion-inducing-cysteine-rich protein with kazal motifs (*RECK*)). Thus, it is reasonable to suggest the modulation of MMPs, TIMPs, and *RECK* in response to LDHs, because they are involved with the development of mineralized tissue.[28–30] Mg–Al LDH promoted a significant upexpression of *MMP9* and *TIMP1*, while *MMP2*, *TIMP2*, and *RECK* remained very similar to the control group (Figure 4c–g). With Zn–Al LDH, there was significant upactivation of *MMP2*, while all those MMP-related inhibitors evaluated here were upmodulated (Figure 4c–g). Differential modulation of ECM remodeling-related genes occurred with both LDHs, which suggests lower activity of MMPs in response to Zn–Al LDH, as all MMP inhibitors were upexpressed, impairing MMP

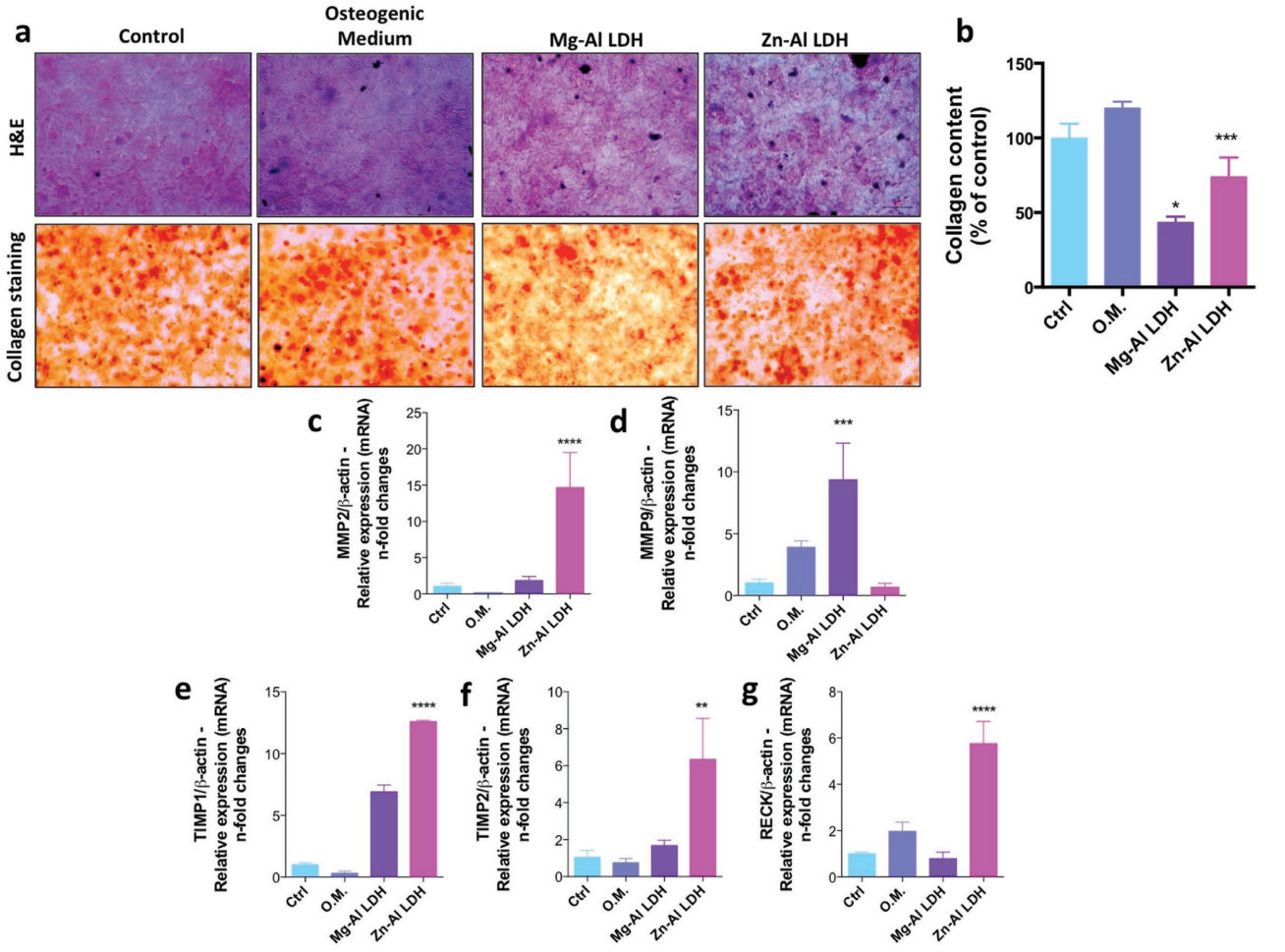

Figure 4. LDHs promote ECM remodeling during osteoblast differentiation. We evaluated ECM remodeling by first staining the cells with a) hematoxylin & eosin and b) collagen fibers (Picro siruis). As ECM-remodeling seemed to be modulated by LDHs, we investigated whether MMPs and their inhibitors were required in response to LDHs. The cells were cultured up to 14 d, when the total mRNA was collected and forwarded to quantitative polymerase chain reaction (qPCR) technology. ECM remodeling-related genes were investigated as follows: c) *MMP2*, d) *MMP9*, e) *TIMP1*, f) *TIMP2*, and g) *RECK*. The ECM-related genes clearly reprogramed in response to both LDHs. *$p < 0.05$; **$p < 0.015$; ***$p < 0.0002$; ****$p < 0.0001$: Significant statistical difference when compared to control.

activities. Thus, this balance of ECM-related gene reprograming may explain the difference of collagen I content response to both LDHs (Figure 4b).

2.4. Both LDH Materials Promoted Expression of Osteogenic Marker Genes

To evaluate osteogenic phenotype, we first found that both evaluated LDH materials could trigger intracellular pathways culminating in osteogenic markers of gene expressions. Both LDH samples promoted a significant increase of *RUNX2* when compared to immediate control, where the cells were cultured at classical condition, and to the positive control (**Figure 5**a), where the cells were incubated with an osteogenic medium (see the Experimental Section for details). In addition, both LDHs upmodulated Osterix expression, when compared to immediate control (Figure 5b), but only Mg_2Al–Cl material promoted a very significant increase, when compared to both listed controls. Similar to *RUNX2* and Osterix, Osteocalcin mRNA was also significantly upexpressed (Figure 5d). Importantly, alkaline phosphatase (*ALP* mRNA) was significantly upmodulated, reaching almost 50-fold increase compared to unchallenged cells (Figure 5c). This result was validated by *ALP* staining (Figure 5i). In addition, Osteopontin (*OPN* mRNA), bone sialoprotein (*BSP* mRNA), bone morphogenetic proteins *(BMP2)*, and *BMP7* genes were investigated. *OPN* mRNA was significantly upmodulated in response to Zn–Al LDH (sixfold changes increase) (Figure 5e). Importantly, *BSP* mRNA emerged as the

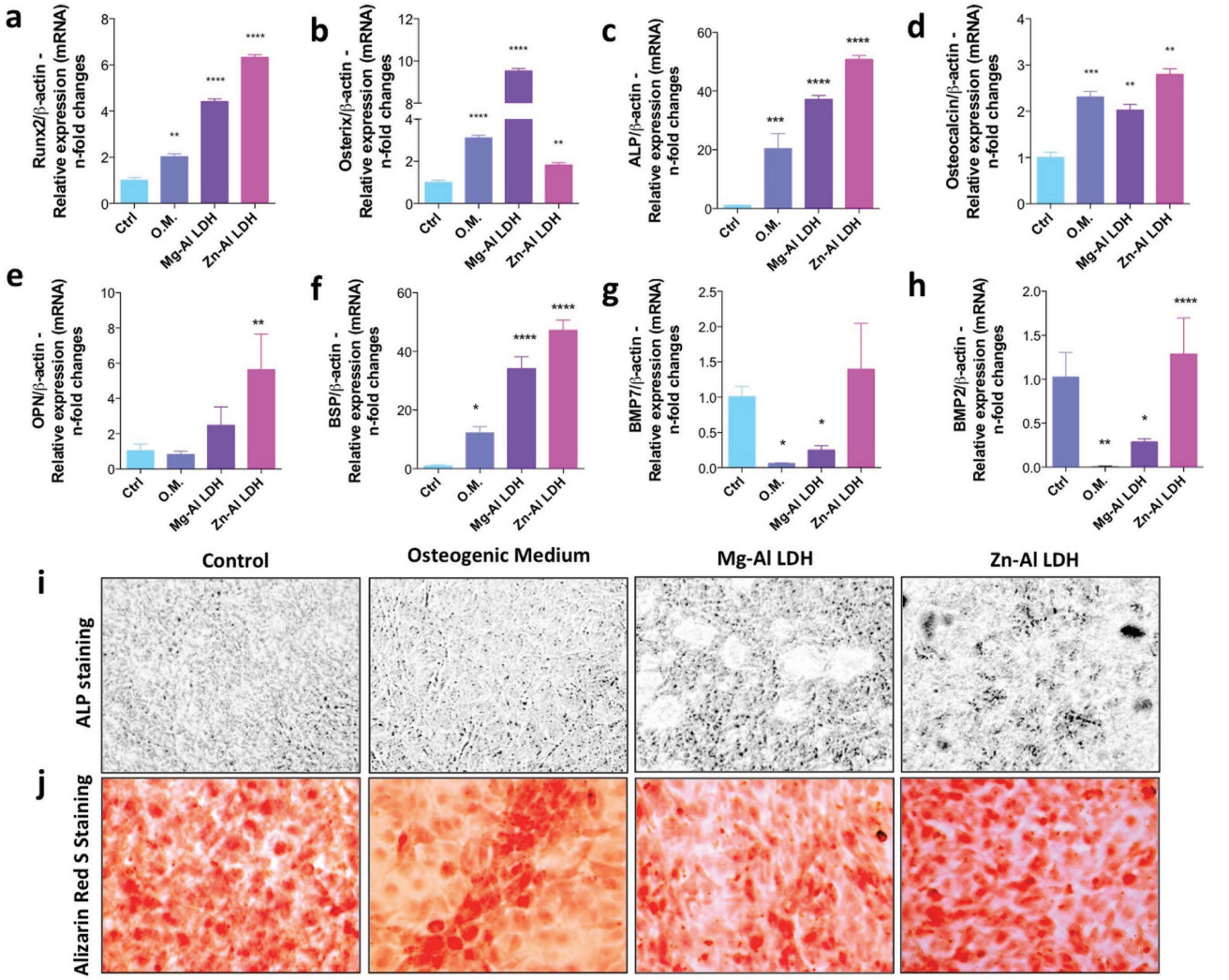

Figure 5. LDHs promote osteoblast differentiation. To evaluate the impact of LDH on osteoblast differentiation, we have added another control group, where the cells were maintained under a classical osteogenic medium treatment [β-Glycerophosphate (10×10^{-3} M) + Dexamethasone (0.03 g mL^{-1}) + ascorbic acid (50 µg mL^{-1})]. The cells were cultured in each experimental condition up to 14 d; then the samples were extracted, cDNA synthesis processed, the expressions of osteogenic markers genes evaluated. a) *RUNX2* upmodulation in response to LDHs, as well as b) Osterix, c) *ALP*, and d) Osteocalcin. Additionally, e) Osteopontin (*OPN*) and f) bone sialoprotein (*BSP*) upmodulated in response to LDHs. Curiously, *BSP* had almost 50-fold greater changes compared to unchallenged cells. In addition, we also investigated whether the BMP-induced autocrine signaling was required by analyzing the activation of g) *BMP2* and h) *BMP7* genes. Complementarily, we subjected challenged cells to *ALP* staining to elucidate i) the distribution of this enzyme and j) mineralization in vitro by Alizarin S Red. *$p < 0.05$; **$p < 0.015$; ***$p < 0.0002$; ****$p < 0.0001$: Significant statistical difference when compared to control.

only bona fide candidate for hydroxyapatite nucleation,[31] and this gene considerably increased in response to LDHs (greater than 40-fold increase for both LDHs) (Figure 5f). Both BMP genes presented very similar profile for both LDHs, which was higher in response to Zn–Al LDH (Figure 5g,h). Curiously, both *BMP2* and *BMP7* mRNAs were downregulated in response to osteogenic medium and Mg–Al LDH, suggesting that there is no a autocrine BMP-induced stimulation of osteoblast differentiation (Figure 5g,h).

In addition, we stained the cells with Alizarin S red to estimate the in vitro mineralization. Our results showed that both LDH materials promoted in vitro mineralization similar to the positive control (Figure 5j). This result reinforces the activity of *BSP* as a mineralizing nucleation protein (Figure 5f).

2.5. LDH Promotes Upexpression of Receptor Activator of NF-KappaB Ligand (*RANKL*) and osteoprotegerin (*OPG*), Which Probably Interfere in Osteoclastogenesis

Hematopoietic cell-derived osteoclasts depend on osteoblast metabolism, largely because osteoblasts express the *RANKL*, which is an essential cytokine for osteoclastogenesis. On the other hand, osteoblasts also produce *OPG*, a decoy receptor for *RANKL*, which inhibits osteoclast differentiation. Thus, the *RANKL*/*RANK*/*OPG* balance is a central axis to modulate osteoclastogenesis.[32] Thus, we are interested whether LDH-challenged osteoblast can modulate both *OPG* and *RANKL* genes. Our results found a dynamic reprograming of both *OPG* mRNA and *RANKL* mRNA in response to both LDHs. Both Mg–Al LDH and Zn–Al LDH promoted a considerable increase on *OPG* expression (**Figure 6**a), which was highest in response to Zn–Al LDH, when compared to control group (Figure 6a). In turn, *RANKL* mRNA was also modulated in response to both LDHs, but only Zn–Al LDH promoted a higher expression than other groups (Figure 6b). Importantly, the chemical-induced osteoblast differentiation by osteogenic medium (here used as a positive control of the osteogenic phenotype) does not seem to contribute to osteoclatogenesis, since both *OPG* mRNA and *RANKL* mRNA were downregulated compared to unchallenged osteoblasts (Figure 6a,b). Figure 6c illustrates the effect of LDH on osteoclastogenesis which stimulates osteoblast upregulation of *RANKL* and *OPG*.

Summarizing, **Figure 7** illustrates the signaling pathways involved in response to LDH by osteoblasts. LDH promotes osteoblastic phenotype by upregulating osteogenic marker genes. In addition, we reported that LDH is an important stimulus for osteoclastogenesis, due to upregulation of *OPG* and *RANKL* expressions. Thus, LDH should be considered in bone disorders.

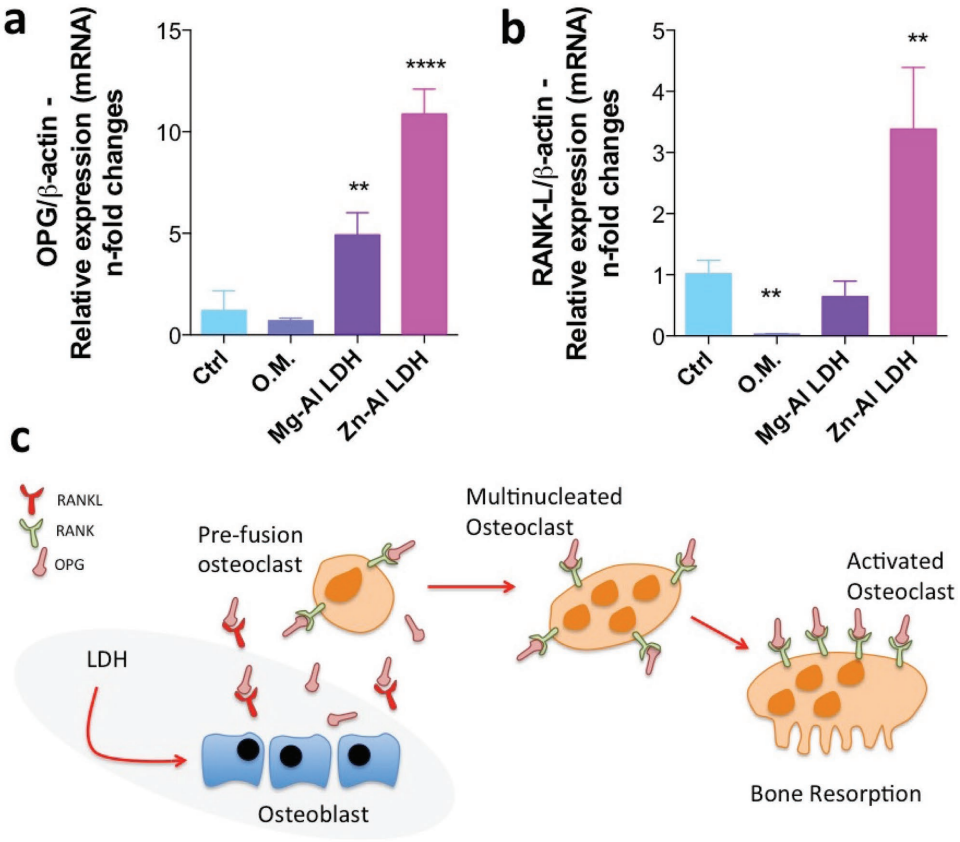

Figure 6. LDHs contribute in osteoblast-induced osteoclastogenesis. LDH-challenged osteoblasts were lysed and the total mRNA collected. After cDNA synthesis processing, the expressions of *RANKL* and *OPG* genes were evaluated. Both LDHs promoted upexpression of a) *OPG*, while *RANKL* was upexpressed only in response to b) Zn–Al LDH. c) *RANKL* and *OPG* are proteins released by osteoblast and related with osteoclastogenesis. $^{**}p < 0.015$; $^{****}p < 0.0001$: Significant statistical difference when compared to control.

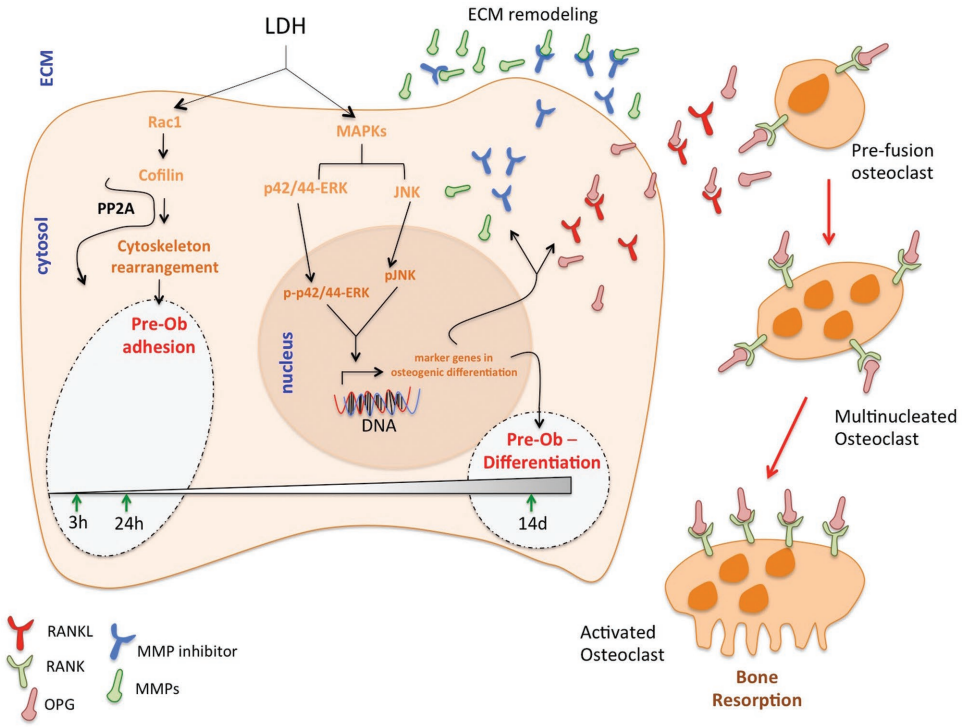

Figure 7. Schematic representation of the LDH-based intracellular signaling. LDHs promoted profound intracellular consequences on preosteoblast (pre-Ob) metabolism interfering in bone remodeling. First, LDHs promoted a significant modulation of cytoskeleton-related proteins, culminating in pre-Ob adhesion up to 24 h as a prerequisite for osteoblast differentiation. In addition, LDHs promote osteogenic phenotype at a MAPK-dependent signaling. As consequences, LDHs promote a dynamic ECM reprograming of remodeling-related genes and also contribute to osteoclastogenesis, since they upmodulate both *RANKL* and *OPG* in challenged osteoblast. The balance of *RANKL* and *OPG* orchestrates the fusion of mononuclear cells, culminating in specialized multinucleated osteoclasts that are responsible for promoting bone resorption. Summarizing, our data showed that LDH has an important effect on bone remodeling because it interferes with osteoblast and osteoclast.

3. Discussion

Novel strategies need to be investigated to clinically regenerate bone when there are critical-sized bone defects. Materials able to repair bone by stimulating an expression of marker genes in osteogenic differentiation are urgently necessary. We addressed this by investigating the effects of LDHs on pre-Ob performance. Immediately after their synthesis and characterization, the LDHs were used to challenge pre-Ob to verify their cytotoxicity, as recommended by ISO 10993-5:2016.

After identifying a safe concentration, we intensified the experiments for possible use in bone scaffold or drug-delivery nanomaterial for bone disorders. In sequence, we showed that LDH interferes pre-Ob adhesion by modulating a crucial intracellular pathway involved with cytoskeleton rearrangement, because important transducers as Rac-1, Cofilin, and PP2A were dynamically modulated. Rac-1 protein decreased in response to both evaluated LDHs, while phosphorylation of Cofilin significantly increased in response to both LDHs, presenting a very similar phosphorylation profile at both 3 and 24 h. This phosphorylation balance of Cofilin can be explained by the strong inactivation of PP2A,[25,33,34] because this Ser/Thr phosphatase was significantly phosphorylated in response to both LDHs. It is very known that PP2A modulates cytoskeleton rearrangement by guiding Cofilin phosphorylation at Serine 03.[35] Elsewhere, we reported that intracellular pathways culminating in cytoskeleton rearrangement are very important to guarantee pre-Ob morphological changes in the beginning of the interaction with the substrate.[36]

After favoring cell adhesion, the promising novel candidates for application in bone disorders need to stimulate the differentiation of pre-Ob into mature osteoblasts. Thus, we investigated if LDH promoted osteoblast differentiation by upmodulating classical marker genes, such as the expression of early marker genes for osteoblast differentiation like *RUNX2* and Osterix (*OSX*) as late marker gene, osteocalcin (*OCN*). Our results found that both LDH materials promoted a significant increase of *RUNX2* and *OCN* when compared to the experimental controls. *OSX* mRNA was also upmodulated by the both LDHs, but Mg_2Al–Cl was more significant compared to the both experimental controls. During the molecular sequence of bone formation, *OSX* is essential for osteoblast differentiation and intramembranous/endochondral bone formation,[37,38] while *RUNX2* is a bone-requisite transcription factor for the maturation of osteoblasts, whereas *OSX* is a downstream gene of *RUNX2*.[39–42] Interestingly, Baek et al.[43] reported that in *OSX*-inactivated adult mice, *RUNX2* expression was significantly increased. Although the exact mechanism is not yet clear, they suggested that the increased *RUNX2* expression may be partly caused by the lack of *OSX*-mediated negative feedback mechanism and its expression may be controlled by the activation of the *OSX*-mediated gene. Therefore, it is reasonable to purpose

that Zn_2Al–Cl LDH interfered with the pre-Ob differentiation by a similar mechanism, as the *RUNX2* mRNA was significantly upexpressed (almost threefold changes compared to control) while *OSX* mRNA was moderately expressed. As reported, bone matrix mineralization is widely regulated by the sequential marker gene expressions, which strictly depends on the stage of osteoblast differentiation. In addition, we subjected the cell to different staining to identify a profile of collagen deposition and late in vitro mineralization by performing Picrosirus and Alizarin S red, respectively. As previously noticed elsewhere, we found a difference in the collagen deposition and mineralization distinguishing both LDHs evaluated in a descriptive and qualitative way. However, other methodologies must be applied for more conclusive explanations of this matter (e.g., members of collagen family and *BSP* expressions by qPCR).

Additionally, investigation of intracellular pathways showed that MAPKs ERK and JNK were required in response to both LDHs, while AKT remained active. It is well-known that MAPK superfamily, including ERKs and JNKs, integrates signals from a wide range of extracellular stimuli, guiding important roles in cellular fate such as proliferation, differentiation, and cell death. For bone, Kim et al.[44] indicated that osteoblast differentiation requires activating ERK and JNK, elucidating the molecular basis of the osteogenic effects of Fucoidan in mesenchyme stem cells; however, the JNK–MAPK pathway is by far the least understood MAPK pathway in osteoblasts, because the bone phenotype of JNK-deficient mice has yet to be reported.[26] The elegant work by Matsuguchi et al.[45] strongly suggests a critical role of JNK in the process of osteoblast differentiation.

MAPKs regulate key transcriptional mediators of osteoblast differentiation, with ERK and p38 MAPKs phosphorylating *RUNX2*, the master regulator of osteoblast differentiation.[26] The domains involved in ERK binding to *RUNX2* have been mapped to a MAPK-binding D-domain, which is the C-terminal proline/serine/threonine-rich domain of *RUNX2*,[46,47] indicating that ERK activity may be differentially regulated in the context of specific osteoblast-relevant promoters. Further work is needed to identify both the range of genes bound by ERK and the functional importance of this association, as suggested by Greenblatt et al..[26]

We showed for the first time that both LDH Mg_2Al–Cl and Zn_2Al–Cl promoted osteoblast differentiation by upmodulating osteoblastic classical marker genes (*RUNX2, OSX*, and *OCN*) by requiring the activation of JNK and ERK, while AKT remained in an active status. Additionally, because adequate osteoblastic differentiation is essential to maintain bone mass through life and strictly necessary for bone healing, LDHs must be explored as therapeutic nanomaterials to be applied into bone disorders as a scaffold for bone bioengineering or as a drug-delivery material to release topically specific molecules that facilitate local bone repair.

4. Experimental Section

Reagents: The antibodies used include Rac1/Cdc42 Antibody (#4651, 21 kDa); Cofilin (D59) Antibody (#3318, 19 kDa); Phospho-Cofilin (Ser3) Antibody (#3311, 19 kDa); glyceraldehyde 3-phosphate dehydrogenase (GAPDH) (14C10) Rabbit mAb (#2118, 37 kDa); AKT Antibody (#9272, 69 kDa); ERK (42, 44 kDa), p-ERK (42, 44 kDa); AKT (#4685, 60 kDa); Phospho-AKT (#4060, 60 kDa)), and JNK (46, 54 kDa) (Phospho-MAPK Family Antibody Sampler Kit #9910). Anti-PP2A alpha + beta antibody (ab137849) was purchased from Abcam (Cambridge, MA, USA) and Anti-PP2A alpha + beta antibody [phospho-Y119] from Cell Signaling (Danvers, MA, USA). All the other chemicals and reagents used in this study were of analytical grade, purchased from commercial sources.

Cell Culture and Conditions: Preosteoblasts were plated on cell-culture dish plates with a density of 25 000 cells cm^{-2} and cultured in minimum essential medium eagle-α modification (α-MEM) until they were confluent. The cells were maintained in osteogenic medium (100 U mL^{-1} penicillin, 100 mg mL^{-1} streptomycin), supplemented with ribonucleosides and deoxyribonucleosides with the addition of β-glycerophosphate (10×10^{-3} M) and ascorbic acid (50 µg mL^{-1}) for αMEM (considered osteogenic medium, O.M.). Cells were cultured for 14 d, with the medium changed every 3 d. Cells were maintained at 37 °C, 5% CO_2, and 95% humidity.

Cell Viability Was Measured by MTT Reduction: Briefly, cells (25 000 cells cm^{-2}) were plated 48 h prior to treatment in a 96-well plate. After 24 h of plating, they were exposed to different concentrations of both LDHs up to 24 h, then the cell viability was assessed by the MTT approach. The cell culture medium was removed, and immediately MTT (1 mg mL^{-1}) was added, and they were kept in an incubator for an additional 4 h. Then, the medium containing MTT was removed and 1 mL of dimethyl sulfoxide was added for solubilization of the blue dye formed by viable cells.[48] Afterward, the absorbance was measured at 570 nm using a microplate reader (SYNERGY-HTX multi-mode reader, Biotek, USA).

Cell Adhesion Was Assayed by Violet Crystal: For the adhesion approach, MC3T3-E1 cells were treated properly with the both LDH samples up to 24 h. Then, the cells were trypsinized, resuspended in conventional medium containing LDH, counted in hematological chamber, and plated (25 000 cells cm^{-2}) in 96-well plates.[49] After plating, cell adhesion was estimated by incorporation of crystal violet dye at the 3 h and 24 h postplating times.

Western Blotting: Respecting the different proposals, after 3 and 24 h for adhesion and 14 d for differentiation, the cells were lysed with Lysis buffer (50×10^{-3} mol L^{-1}, Tris-HCl, pH 7.4, 1% Tween 20, 0.25% sodium deoxycholate, 150×10^{-3} mol L^{-1} NaCl, 1×10^{-3} mol L^{-1} ethylene glycol tetraacetic acid (EGTA), 1×10^{-3} mol L^{-1} *O*-Vanadate, 1×10^{-3} mol L^{-1} NaF, and protease inhibitors 10 µg mL^{-1} leupeptin and 1×10^{-3} mol L^{-1} 4-aminoethyl fluorosulfonyl 4-hydrochloride hydrochloride). The samples were sonicated (1 pulse s^{-1}, in a SONICS Vibra-Cell equipment) and maintained for 1 h on ice, when in each sequential 20 min, the samples were vortexed. Then, protein extracts were pooled by centrifuging (14 000 rpm) and the protein amount determined by the Lowry method.[50] Finally, the protein extracts were added of 2× Laemmli buffer [2× sodium dodecyl sulfate (SDS), 100×10^{-3} mol L^{-1} Tris-HCl [pH 6.8], 200×10^{-3} mol L^{-1} dithiothreitol (DTT), 4% SDS, 0.1% bromophenol blue, and 20% glycerol], and maintained for 5 min at 95 °C. Once prepared, the samples were resolved on sodium dodecyl sulphate-polyacrylamide gel electrophoresis (SDS-PAGE) gel.

Osteogenic Phenotype: The osteogenic classical marker genes were analyzed by qPCR. For expression analysis, TriZol was added to the cultures and pelleted. After centrifugation, addition of chloroform and centrifugation, DNA, RNA, and protein phases were formed in the tube. RNA samples were quantified using plate reader (SYNERGY-HTX multi-mode reader, Biotek, USA). The next step was cDNA synthesis using the High-Capacity cDNA Reverse Transcription Kit – Applied Biosystems [2.0 µL of 10× RT Buffer, 0.8 µL 25× dNTP Mix (100×10^{-3} mol L^{-1}), 2.0 µL 10× RT Randon Primers, 1.0 µL MultiScrible Reverse Transcriptase, 4.2 µL Nuclease-Free H_2O], then 200 ng μL^{-1} of each sample was added for cDNA synthesis in a 96-well plate and taken to the QuantStudio 3 (Applied Biosystems). After this initial process, the material was collected and evaluated for the expression (**Table 1**). In addition, histochemical staining for *ALP* activity in the cells was determined using Sigma Fast BCIP/NBT Tablets (B5655) according to the manuals.

In Vitro Picrosirius Staining: Preosteoblasts were plated at a density of 8×10^4 cells mL^{-1} in 24-well plates and in semiconfluence treated

Table 1. Expression primer sequences and PCR cycle conditions.

Gene	Primer	5′–3′ Sequence	Reaction condition
MMP2	Forward	AACTTTGAGAAGGATGGCAAGT	95 °C – 3 s; 60 °C – 8 s; 72 °C – 20 s
	Reverse	TGCCACCCATGGTAAACAA	
MMP9	Forward	TGTGCCCTGGAACTCACACGAC	95 °C – 3 s; 62 °C – 8 s; 72 °C – 20 s
	Reverse	ACGTCGTCCACCTGGTTCACCT	
TIMP1	Forward	ATCCTCTTGTTGCTATCACTG	95 °C – 5 s; 60 °C – 10 s; 72 °C – 15 s
	Reverse	GGTCTCGTTGATTTCTGGG	
TIMP2	Forward	GCAACAGGCGTTTTGCAATG	95 °C – 3 s; 60 °C – 8 s; 72 °C – 20 s
	Reverse	CGGAATCCACCTCCTTCTCG	
RECK	Forward	CCTCAGTGAGCACAGTTCAGA	95 °C – 3 s; 60 °C – 8 s; 72 °C – 20 s
	Reverse	CCTGTGGCATCCACGAAACT	
Col 1A1	Forward	ATGACGTGATCTGTGACGAGAC	95 °C – 3 s; 62 °C – 8 s; 72 °C – 20 s
	Reverse	TTCTTGGTCGGTGGGTGAC	
Col 3A1	Forward	GACCTGAAATTCTGCCATCC	95 °C – 3 s; 62 °C – 8 s; 72 °C – 20 s
	Reverse	GCATGTTTCCCCAGTTTCC	
BSP	Forward	GTACCGGCCACGCTACTTTCT	95 °C – 3 s; 60 °C – 8 s; 72 °C – 20 s
	Reverse	GTTGACCGCCAGCTCGTTTT	
BMP2	Forward	GGTCACAGATAAGGCCATTGC	95 °C – 3 s; 60 °C – 8 s; 72 °C – 20 s
	Reverse	GCTTCCGCTGTTTGTGTTTG	
BMP7	Forward	TGACAAAGAATTCTTCCACCCTCGA	95 °C – 5 s; 72 °C – 10 s; 72 °C – 15 s
	Reverse	GTAATACGACTCACTATAGGGCAGGGTTGCTTGTTCTGGGGT	
OPG	Forward	CAGAGACTAATAGATCAAAGGCAGG	95 °C – 3 s; 60 °C – 8 s; 72 °C – 20 s
	Reverse	ATGAAGTCTCACCTGAGAAGAACC	
RANKL	Forward	CGCTCTGTTCCTGTACTTTCGAGCG	95 °C – 3 s; 60 °C – 8 s; 72 °C – 20 s
	Reverse	TCGTGCTCCCTCCTTTCATCAGGTT	
RUNX2	Forward	GGACGAGGCAAGAG 1 II CA	95 °C – 3 s; 55 °C – 8 s; 72 °C – 20 s
	Reverse	TGGTGCAGAGTTCAGGGAG	
ALP	Forward	GAAGTCCGTGGGCATCGT	95 °C – 3 s; 55 °C – 8 s; 72 °C – 20 s
	Reverse	CAGTGCGGTTCCAGACATAG	
Osteocalcin (*OCN*)	Forward	AGACTCCGGCGCTACCTT	95 °C – 3 s; 55 °C – 8 s; 72 °C – 20 s
	Reverse	CTCGTCACAAGCAGGGTTAAG	
Osterix (*OSX*)	Forward	CCC TTC CCT CAC TCA TTT CC	95 °C – 5 s; 56 °C – 10 s; 72 °C – 15 s
	Reverse	CAA CCG CCT TGG GCT TAT	
Osteopontin	Forward	TTTGCTTTTGCCTGTTTGGC	95 °C – 5 s; 60 °C – 10 s; 72 °C – 15 s
	Reverse	CAGTCACTTTCACCGGGAGG	
β-actin	Forward	TCTTGGGTATGGAATCCTGTG	95 °C – 3 s; 55 °C – 8 s; 72 °C – 20 s
	Reverse	AGGTCTTTACGGATGTCAACG	

with the different LDH materials up to 14 d. For qualitative analysis of collagen content, the cells were washed in phosphate buffered saline (PBS) and fixed in 4% paraformaldehyde for 1 h and then stained for 90 min in a 0.1% solution of red Sirius in saturated aqueous picric acid, pH 2. Next, the cells were washed for 2 min in 0.01 N HCl and counterstained with Harris Hematoxylin for 6 min, washed in ethanol 70%, dehydrated, and mounted using Permount. For the conventional fluorescence microscope, images were acquired in the inverted microscope Axio Vert.A1 (Zeiss, Germany).

In Vitro Hematoxylin & Eosin Staining: Preosteoblasts were plated at a density of 8×10^4 cells mL^{-1} in 24-well plates and in semiconfluence treated with the different LDH materials up to 14 d. For a morphological analysis of the cells, hematoxylin & eosin technology was used, where the cells were previously fixed in phosphate-buffered 4% paraformoldehyde for 40 min, washed with water for 7 min, incubated for 5 min in hematoxylin, washed with water for 3 min, and stained with eosin for 7 min. Then, the coverslips were dehydrated and photographed under a conventional optical microscope Axio Vert.A1 (Zeiss, Germany).

In Vitro Alizarin S Red Staining: Preosteoblasts were plated at a density of 8×10^4 cells mL^{-1} in 24-well plates and in semiconfluence treated with the different LDH materials, as previously described, up to 14 d. The medium was changed every 3 d. In vitro mineralization was measured during osteoblast differentiation process by alizarin Red S staining. The culture medium was gently removed and washed with warm PBS.

Thereafter, the PBS was removed, and 0.5 mL of 10% formalin was added for cell fixation. The plate was held in that solution for 30 min at room temperature. After this period, formalin was removed, and Alizarin solution (1%) added in the cultures, and then they were incubated in the dark chamber for additional 45 min. The cells were washed five times in PBS. Finally, cell images were acquired by using an inverted microscope (Zeiss, Germany).

Statistical Analysis: Results were plotted as mean ± standard deviation and verified using one-way analysis of variances (ANOVA) (nonparametric) with Tukey's post-test, to compare all pairs of groups. In this case, $p < 0.05$ was considered statistically significant and $p < 0.0001$ considered highly significant. The software used was GraphPad Prism 6. For particle counting, ImageJ Software was used to determine the number of points in the area recorded in the photo, and for the statistical analysis, the groups were standardized by the percentage of the control.

Acknowledgements

The authors would like to thank the FAPESP (Proc. 2014/22689-3; 2011/50318-1) and the CNPq for the financial support. The authors are thankful to Dr. Vanessa R. R. Cunha for preparation of samples.

Conflict of Interest

The authors declare no conflict of interest.

Keywords

differentiation, double metal hydroxides, hydrotalcite-like materials, layered double hydroxides, nanoparticles, osteoblasts

Received: June 2, 2017
Revised: October 14, 2017
Published online: December 27, 2017

[1] S. Gemini-Piperni, E. R. Takamori, S. C. Sartoretto, K. B. S. Paiva, J. M. Granjeiro, R. C. de Oliveira, W. F. Zambuzzi, *Arch. Biochem. Biophys.* **2014**, *561*, 88.
[2] A. Teti, *Curr. Osteoporosis Rep.* **2011**, *9*, 264.
[3] S. Yazar, C.-H. Lin, F.-C. Wei, *Plast. Reconstr. Surg.* **2004**, *114*, 1457.
[4] P. Habibovic, K. de Groot, *J. Tissue Eng. Regener. Med.* **2007**, *1*, 25.
[5] A. Del Fattore, A. Teti, N. Rucci, *Front. Biosci., Elite Ed.* **2012**, *4*, 2302.
[6] A. Marumoto, R. Milani, R. A. da Silva, C. J. da Costa Fernandes, J. M. Granjeiro, C. V. Ferreira, M. P. Peppelenbosch, W. F. Zambuzzi, *Bone* **2017**, *103*, 55.
[7] C. J. Serna, J. L. White, S. L. Hem, *J. Pharm. Sci.* **1978**, *67*, 324.
[8] K. H. Holtermuller, M. Liszkay, I. Bernard, W. Haase, *Z. Gastroenterol.* **1992**, *30*, 717.
[9] A. Tarnawski, R. Pai, R. Itani, F. A. Wyle, *Digestion* **1999**, *60*, 449.
[10] A. S. Tarnawski, M. Tomikawa, M. Ohta, I. J. Sarfeh, *J. Physiol.* **2000**, *94*, 93.
[11] Z. Gu, J. J. Atherton, Z. P. Xu, *Chem. Commun.* **2015**, *51*, 3024.
[12] S.-J. Choi, J.-H. Choy, *Nanomedicine* **2011**, *6*, 803.
[13] R. Liang, M. Wei, D. G. Evans, X. Duan, *Chem. Commun.* **2014**, *50*, 14071.
[14] B. Saifullah, M. Z. B. Hussein, *Int. J. Nanomed.* **2015**, *10*, 5609.
[15] Y. Kuthati, R. K. Kankala, C.-H. Lee, *Appl. Clay Sci.* **2015**, *112*, 100.
[16] V. R. R. Cunha, P. A. D. Petersen, M. B. Gonçalves, H. M. Petrilli, C. Taviot-Gueho, F. Leroux, M. L. A. Temperini, V. R. L. Constantino, *Chem. Mater.* **2012**, *24*, 1415.
[17] O. M. Gil, M. A. Rocha, V. R. L. Constantino, I. H. J. Koh, D. L. A. de Faria, *Vibrational Spectroscopy* **2016**, *87*, 60.
[18] M. A. Rocha, P. A. D. Petersen, E. Teixeira-Neto, H. M. Petrilli, F. Leroux, C. Taviot-Guehode, V. R. L. Constantino, *RSC Adv.* **2016**, *6*, 16419.
[19] V. R. R. Cunha, V. A. Guilherme, E. de Paula, D. R. de Araujo, R. O. Silva, J. V. R. Medeiros, J. R. S. A. Leite, P. A. D. Petersen, M. Foldvari, H. M. Petrilli, *Mater. Sci. Eng., C* **2016**, *58*, 629.
[20] V. R. R. Cunha, R. B. de Souza, A. M. C. R. P. da Fonseca Martins, I. H. J. Koh, V. R. L. Constantino, *Sci. Rep.* **2016**, *6*, 30547.
[21] G. Kapusetti, R. R. Mishra, S. Srivastava, N. Misra, V. Singh, P. Roy, S. K. Singh, C. Chakraborty, S. Malik, P. Maiti, *J. Mater. Chem. B* **2013**, *1*, 2275.
[22] Y.-X. Chen, R. Zhu, Z. Xu, Q.-F. Ke, C.-Q. Zhang, Y.-P. Guo, *J. Mater. Chem. B* **2017**, *5*, 2245.
[23] S. Bertazzo, W. F. Zambuzzi, D. D. P. Campos, C. V. Ferreira, C. A. Bertran, *Clin. Oral Implants Res.* **2010**, *21*, 1411.
[24] S. Bertazzo, W. F. Zambuzzi, D. D. P. Campos, T. L. Ogeda, V. Ferreira C, C. A. Bertran, *Colloids Surf., B* **2010**, *78*, 177.
[25] W. F. Zambuzzi, A. Bruni-Cardoso, J. M. Granjeiro, M. P. Peppelenbosch, H. F. de Carvalho, H. Aoyama, C. V. Ferreira, *J. Cell. Biochem.* **2009**, *108*, 134.
[26] M. B. Greenblatt, J.-H. Shim, L. H. Glimcher, *Annu. Rev. Cell Dev. Biol.* **2013**, *29*, 63.
[27] P. Lu, K. Takai, V. M. Weaver, Z. Werb, *Cold Spring Harbor Perspect. Biol.* **2011**, *3*, 12.
[28] A. C. C. de Oliveira Demarchi, W. F. Zambuzzi, K. B. S. Paiva, M. D. G. da Silva-Valenzuela, F. D. Nunes, R. D. C. S. Figueira, R. M. Sasahara, M. A. A. Demasi, S. M. B. Winnischofer, M. C. Sogayar, J. M. Granjeiro, *Cell Tissue Res.* **2010**, *340*, 61.
[29] W. F. Zambuzzi, C. L. Yano, A. D. M. Cavagis, M. P. Peppelenbosch, J. M. Granjeiro, C. V. Ferreira, *Mol. Cell. Biochem.* **2009**, *322*, 143.
[30] K. B. S. Paiva, W. F. Zambuzzi, T. Accorsi-Mendonca, R. Taga, F. D. Nunes, M. C. Sogayar, J. M. Granjeiro, *J. Mol. Histol.* **2009**, *40*, 201.
[31] B. Ganss, R. H. Kim, J. Sodek, *Crit. Rev. Oral Biol. Med.* **1999**, *10*, 79.
[32] Y. Kobayashi, N. Udagawa, N. Takahashi, *Crit. Rev. Eukaryotic Gene Expression* **2009**, *19*, 61.
[33] N. V. Oleinik, N. I. Krupenko, S. A. Krupenko, *Oncogene* **2010**, *29*, 6233.
[34] A. Blangy, H. Touaitahuata, G. Cres, G. Pawlak, *PLoS One* **2012**, *7*, e45909.
[35] W. F. Zambuzzi, C. V. Ferreira, J. M. Granjeiro, H. Aoyama, *J. Biomed. Mater. Res., Part A* **2011**, *97*, 193.
[36] S. Gemini-Piperni, R. Milani, S. Bertazzo, M. Peppelenbosch, E. R. Takamori, J. M. Granjeiro, C. V. Ferreira, A. Teti, W. F. Zambuzzi, *Biotechnol. Bioeng.* **2014**, *111*, 1900.
[37] J. Lu, S. Qu, B. Yao, Y. Xu, Y. Jin, K. Shi, Y. Shui, S. Pan, L. Chen, C. Ma, *Oncotarget* **2016**, *7*, 37471.
[38] A. M. Buo, R. E. Tomlinson, E. R. Eidelman, M. Chason, J. P. Stains, *J. Bone Miner. Res.* **2017**, *32*, 1727.
[39] C. A. Yoshida, H. Yamamoto, T. Fujita, T. Furuichi, K. Ito, K. Inoue, K. Yamana, A. Zanma, K. Takada, Y. Ito, T. Komori, *Genes Dev.* **2004**, *18*, 952.
[40] J. Y. Choi, J. Pratap, A. Javed, S. K. Zaidi, L. Xing, E. Balint, S. Dalamangas, B. Boyce, A. J. V. Wijnen, J. B. Lian, J. L. Stein, S. N. Jones, G. S. Stein, *Proc. Natl. Acad. Sci. USA* **2001**, *98*, 8650.
[41] J. E. Aubin, E. Bonnelye, *Medscape Womens Health* **2000**, *5*, 5.
[42] T. Komori, *J. Cell. Biochem.* **2005**, *95*, 445.
[43] W. Y. Baek, M. A. Lee, J. W. Jung, S. Y. Kim, H. Akiyama, B. de Crombrugghe, J. E. Kim, *J. Bone Miner. Res.* **2009**, *24*, 1055.
[44] B. S. Kim, H. J. Kang, J. Y. Park, J. Lee, *Exp Mol Med.* **2015**, *47*, e128.

[45] T. Matsuguchi, N. Chiba, K. Bandow, K. Kakimoto, A. Masuda, T. Ohnishi, *J. Bone Miner. Res.* **2009**, *24*, 398.
[46] C. Ge, Q. Yang, G. Zhao, H. Yu, K. L. Kirkwood, R. T. Franceschi, *J. Bone Miner. Res.* **2012**, *27*, 538.
[47] G. Xiao, D. Jiang, R. Gopalakrishnan, R. T. Franceschi, *J. Biol. Chem.* **2002**, *277*, 36181.
[48] T. Mosmann, *J. Immunol. Methods* **1983**, *65*, 55.
[49] F. Bezerra, M. R. Ferreira, G. N. Fontes, C. J. da Costa Fernandes, D. C. Andia, N. C. Cruz, R. A. da Silva, W. F. Zambuzzi, *Biotechnol. Bioeng.* **2017**, *114*, 1888.
[50] E. C. Lowry, J. M. Blumberg, R. L. Rhea, J. P. Ranson, *U. S. Armed Forces Med. J.* **1951**, *2*, 265.